



## Thin and flexible all-solid supercapacitor prepared from novel single wall carbon nanotubes/polyaniline thin films obtained in liquid–liquid interfaces



Victor Hugo Rodrigues de Souza <sup>a</sup>, Marcela Mohallem Oliveira <sup>b</sup>,  
Aldo José Gorgatti Zarbin <sup>a,\*</sup>

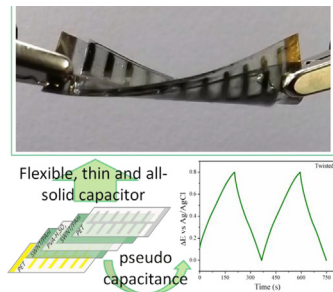
<sup>a</sup> Departamento de Química, Universidade Federal do Paraná (UFPR), Curitiba, Paraná, Brazil

<sup>b</sup> Departamento Acadêmico de Química e Biologia, Universidade Tecnológica Federal do Paraná (UTFPR), Curitiba, Paraná, Brazil

### HIGHLIGHTS

- Flexible, transparent, ITO-free and all solid supercapacitor.
- Excellent performance and improved stability under bending.
- Active layer based on thin films (approximately 120 nm) prepared in an innovative way.
- Complex material for electrochemical energy systems prepared in liquid–liquid interfaces.

### GRAPHICAL ABSTRACT



### ARTICLE INFO

#### Article history:

Received 18 October 2013

Received in revised form

17 February 2014

Accepted 19 February 2014

Available online 12 March 2014

#### Keywords:

Flexible supercapacitor

Pseudo-capacitor

Carbon nanotubes

Polyaniline

Liquid–liquid interfaces

Nanocomposites

### ABSTRACT

The present work describes for the first time the synthesis and characterization of single wall carbon nanotubes/polyaniline (SWNTs/PAni) nanocomposite thin films in a liquid–liquid interface, as well as the subsequent construction of a flexible all-solid supercapacitor. Different SWNTs/PAni nanocomposites were prepared by varying the ratio of SWNT to aniline, and the samples were characterized by scanning and transmission electron microscopy, Raman and UV–Vis spectroscopy, cyclic voltammetry and electrochemical impedance spectroscopy. The pseudo-capacitive behavior of the nanocomposites was evaluated by charge/discharge galvanostatic measurements. The presence of the SWNTs affected the electronic and vibrational properties of the polyaniline and also improved the pseudo-capacitive behavior of the conducting polymer. A very thin and flexible all-solid device was manufactured using two electrodes (polyethylene terephthalate–PET covered with the SWNT/PAni nanocomposite separated by a H<sub>2</sub>SO<sub>4</sub>–PVA gel electrolyte). The pseudo-capacitive behavior was characterized by a volumetric specific capacitance of approximately 76.7 F cm<sup>−3</sup>, even under mechanical deformation, indicating that this nanocomposite has considerable potential for application in new-generation energy storage devices.

© 2014 Elsevier B.V. All rights reserved.

### 1. Introduction

In recent years, the development of energy storage technology has become very important as clean energy generation from flexible, thin and lightweight devices has been developed. Supercapacitors are highly promising candidates to fulfill these energy

\* Corresponding author. Departamento de Química-UFPR, Centro Politécnico, Jardim das Américas, CP 19081, CEP 81531-990 Curitiba, PR, Brazil. Tel./fax: +55 41 33613176.

E-mail addresses: [aldozarbin@ufpr.br](mailto:aldozarbin@ufpr.br), [aldo@pq.cnpq.br](mailto:aldo@pq.cnpq.br) (A.J.G. Zarbin).

storage requirements, as these devices combine the high storage capacity of batteries along with the fast and efficient energy release of capacitors [1]. Supercapacitors can be divided in two types: the double-layer capacitor and the pseudo-capacitor, which differ strictly in their charge storage mode. In the double-layer capacitor, the capacitance results from the separation of charges, being purely electrostatic. Meanwhile, in the pseudo-capacitor, the capacitance results from a Faradaic process, meaning that the storage occurs in response to a redox reaction [1,2].

Carbon-based materials, conducting polymers and metal oxides are broadly applied singly or as composites in the development of supercapacitors. As carbonaceous materials, single wall carbon nanotubes (SWNTs), which generally present double-layer capacitive behavior, are powerful materials that are applied as electrodes for supercapacitors due to their desirable properties such as high surface area, porosity and electrical conductivity [3,4]. Polyaniline (PAni), a conducting polymer with capacitive properties from a Faradaic process, is another material widely applied as a supercapacitor due to its unique properties such as environmental stability, facile preparation, high doping level and fairly high conductivity [2,5,6]. The charge is stored from the redox process of the polyaniline into its different forms (e.g., the transition from the leucoemeraldine to the emeraldine form), which is accompanied by the intercalation and depletion of the counter ions. Besides the conducting polymers as polyaniline, several metal oxides present pseudocapacitive behavior from Faradaic process, being the RuO<sub>2</sub> the most promissory material due to the high specific capacitance and good electronic conductivity [7]. Meanwhile, compared to the metal oxides, the conducting polymers are advantageous due to easiness in synthesis and flexibility [8].

The combination of carbon nanomaterials (such as CNTs) with electroactive materials (conducting polymers/metal oxides) is widely studied. The addition of RuO<sub>2</sub> in a CNTs matrix provided a significant increase in the specific capacitance [7]. CNTs/PAni nanocomposites obtained by chemical [9,10] and electrochemical [11] methods of aniline polymerization has proven very successful in achieving high values of capacitance. The reasons for such performances of CNTs/PAni nanocomposites are the increase of the polyaniline stability due to the presence of the CNTs, the formation of a porous network that provides electrolyte permeation through the entire sample and the enhancement in the conductivity and charge-transfer behavior of the conducting polymer [11,12].

In addition to the synthesis of thin and easily handled nanocomposites for applications in capacitors, the modern market demand is driving the production of flexible, lightweight and all-solid devices capable of retaining pseudo-capacitive behavior even under mechanical deformation. The construction of a flexible, simple and safe device is possible using an all-solid capacitor when the liquid electrolyte generally used in conventional devices is replaced with a gel electrolyte. Recently, many efforts have been made in the development of all-solid devices from carbon nanotubes and polyaniline [13–16], in addition to other capacitors with different capacitive materials, gel electrolytes and device configuration [17–21]. Meanwhile, the fabrication of an all-solid pseudo-capacitor from a thin, flexible and freestanding CNT/PAni nanocomposite has not yet been reported.

Even though several reported composites present impressive values of specific capacitance, most of them display some type of limitation in their processability, requiring multiple steps for the conversion of the nanocomposites to films, the use of external matrices for the nanocomposite deposition during synthesis, as in the case of buckypaper-like devices [15], or a previous synthesis of CNT films for the electrochemical deposition of PAni [11]. Hence, the development of a completely new method to obtain a nanocomposite in a single step is extremely interesting. Our previous

report showed, for the first time, the synthesis and characterization of multi-walled carbon nanotubes/polyaniline (MWNTs/PAni) nanocomposites as thin films from the interfacial method [22], and its utilization as transparent and flexible electrodes in a solar cell [23]. This method was further extended to graphene/polyaniline nanocomposites [24] and also enables the synthesis of nanocomposites using SWNTs, which have displayed superior features as capacitors compared with MWNTs, due to their desirable properties such as high surface area and electrical conductivity.

The present work reports three main goals: the synthesis of SWNTs/PAni nanocomposites as thin and freestanding films in a liquid–liquid interface; the deposition of these films over flexible substrates for the construction of all-solid capacitors; and the characterization of both the nanocomposites and the device.

## 2. Experimental section

The SWNTs (Unydim-HiPCO) with a diameter of 0.8–1.2 nm and a length of 100–1000 nm were used as received. Aniline (Acros) was distilled twice before use. Chloroform (Biotec), toluene (Carlo Erba), sulfuric acid (Carlo Erba) and ammonium persulfate (Acros) were used as received. All solutions were prepared in deionized water (Milli-Q Ultra-Pure-Water Purification System).

The SWNT/PAni nanocomposite films were synthesized by a liquid–liquid interfacial polymerization, adapted from our previous report [22]. All reagent amounts are summarized in Table 1. Firstly, a SWNT dispersion in chloroform (3.12 mg L<sup>−1</sup>) was prepared using an ultrasonic probe system with 40% amplitude for 10 min (Cole-Palmer ultrasonic processor). The dispersion was maintained in an ice-bath to avoid solvent evaporation. The aniline was added to the dispersion, and subsequently, the resulting mixture was transferred to a round-bottom flask containing ammonium persulfate (APS) previously dissolved in 30 mL of a 1 mol L<sup>−1</sup> H<sub>2</sub>SO<sub>4</sub> aqueous solution. The resulting system was maintained under magnetic stirring (approximately 750 rpm) for 22 h at room temperature. Afterward, the magnetic stirring was stopped, and a thin and freestanding film was formed at the chloroform/water interface. The aqueous phase was removed and renewed several times with a H<sub>2</sub>SO<sub>4</sub> (pH 3) aqueous solution until this pH was reached to remove excess of acid. The organic phase was also removed and renewed three times to remove any side products. Finally, the chloroform was changed by toluene to facilitate the removal of the interfacial film. The two-phase system containing the nanocomposite film was transferred to a beaker containing a substrate (the synthesis and film removal are presented in Fig. S1). The substrate was removed using tweezers, and the interfacial film was deposited over it. Neat SWNT and PAni (in the same ratio of aniline in the SWNTs/PAni 1:96 nanocomposite) films were also synthesized following the same procedure described above. The SWNTs/PAni 1:96 nanocomposites and raw PAni with 2 and 3 layers were prepared. Firstly, one layer of nanocomposite (or raw PAni) was deposited over the substrate, as

**Table 1**  
Experimental data for the different samples synthesized.

Sample	Mass of CNT (mg)	Volume of aniline (μL)	Mass of APS (mg)
SWNT	0.1	—	—
SWNT/PAni 1:16	0.1	1.6	1.02
SWNT/PAni 1:96	0.1	9.6	6.12
SWNT/PAni 1:144	0.1	14.4	9.19
PAni	—	9.6	6.12
MWNT <sub>commercial</sub> /PAni	0.1	9.6	6.12
MWNT-Fe/PAni	0.16 <sup>a</sup>	9.6	6.12

<sup>a</sup> Considering 37.2% of Fe-species residue.

illustrated in **Fig. S1**. Next, the substrate was maintained for 30 min at 80 °C, and a subsequent other layer was deposited following the same procedure. The deposition of the third layer also followed the same methodology. For comparison, other composites were synthesized using commercial multiwall carbon nanotubes (NANOCYL-CCVD) with an average diameter of approximately 9.5 nm and a length of 1500 nm, as well as using a home-made multiwall carbon nanotubes filled with iron species (Fe-MWNTs) [25] with a diameter of approximately 70 nm and an average length of 2000 nm, maintaining the same proportion of carbon and aniline in the SWNTs/PAni 1:96 nanocomposite.

An all-solid, highly flexible pseudo-capacitor was fabricated from the SWNT/PAni 1:96 nanocomposite as follows. First, the nanocomposite (synthesized as described before) was deposited over a flexible substrate (PET covered with a chromium/gold layer for electric contact). Then, the two substrates were immersed in a H<sub>2</sub>SO<sub>4</sub>-PVA (polyvinyl alcohol) gel electrolyte [13], removed and dried for 30 min at 35 °C. Afterward, one of the electrodes was immersed again in the gel electrolyte, removed and pressed over another dried electrode. The new device was dried for 30 min at 35 °C, resulting in a pseudo-capacitor with a thin separating layer of H<sub>2</sub>SO<sub>4</sub>-PVA gel electrolyte.

The morphology and the structure of the SWNT/PAni nanocomposites and the raw films were characterized by scanning electron microscopy (SEM-FEG/Tescan) and transmission electron microscopy (TEM, JEOL JEM 120 KV instrument). The images were recorded directly from the films previously deposited over silicon oxide and standard copper grids, respectively.

The electronic structure was characterized by UV–Vis spectroscopy (Shimadzu UV-2450 spectrophotometer). The spectra of the composites were recorded over quartz substrates.

Raman spectra (Renishaw Raman Image spectrophotometer) were acquired using an excitation line of 1.96 eV (632.8 nm/He-Ne laser).

All of the electrochemical characterization was recorded using an Autolab potentiostat (Eco-Chimie) that was interfaced to a PC with GPES 4.9 software. The conventional three-electrode cell consisted of the films (active area = 1.5 × 0.5 cm) deposited over fluorine-doped tin oxide glass as the working electrode, Pt wire as

the counter electrode and Ag/AgCl as the reference electrode. The electrolyte was a 1 mol L<sup>-1</sup> H<sub>2</sub>SO<sub>4</sub> aqueous solution. Cyclic voltammetry (CV) was recorded in the range of 0.2–0.95 V at a scan speed of 20 mV s<sup>-1</sup>. The galvanostatic charge/discharge measurements of the films were recorded in the voltage range of 0–0.6 V at 10.82 μA.

The all-solid pseudo-capacitor was characterized by CV in a range of 0–0.8 V at a scan speed of 10 mV s<sup>-1</sup>, connecting the working electrode to one of the electrodes and the counter electrode along with the reference to another electrode. The same configuration was used for the galvanostatic charge/discharge measurements over a voltage range of 0–0.8 V at 10.82 μA and the stability was set between 0 and 0.5 V during 1000 cycles.

The electrochemical impedance spectroscopy (EIS) was performed using the NOVA software in a range of 10<sup>4</sup> to 10<sup>-2</sup> Hz with amplitude of 10 mV. The equivalent circuit was generated using the ZView software.

The thickness of the films was measured using a Dektak 150 Veeco surface profilometer with a 0.1 μm resolution and 1 mg of probe strength.

### 3. Results and discussion

**Fig. 1** shows the SEM images recorded for the SWNT, PAni and the nanocomposite films deposited over silicon oxide. The presence of rough and uniform aggregates of nanofibers is dominant in the morphology of the neat PAni (**Fig. 1(a)**). In some regions of the film, it is possible to estimate the diameter of the nanofibers, which is approximately 50 nm. The formation of fibers is characteristic for PAni obtained by interfacial polymerization [26–28]. A network of interconnected small bundles of SWNTs can be observed in **Fig. 1(b)**. The SWNTs are randomly arranged in a monolayer of carbon nanotubes, and the diameter of the bundles is approximately 10–50 nm. The morphology of the nanocomposites is directly related to the SWNTs/aniline ratio (**Fig. 1(c)–(e)**). At low SWNTs/PAni ratios (**Fig. 1(c)**), an array of well-distributed SWNT bundles covered with a thin layer of polyaniline is observed. When the aniline ratio is increased, the small polyaniline nanofibers preferentially covering the carbon nanotubes (**Fig. 1(d)**) are

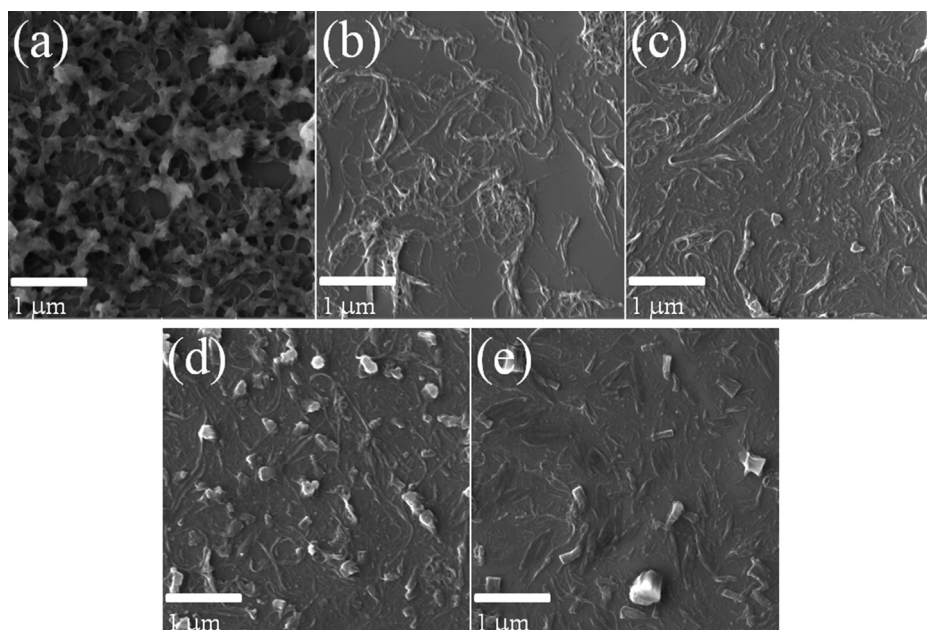


**Fig. 1.** SEM images of the samples: (a) neat PAni; (b) SWNT; (c) SWNT/PAni 1:16; (d) SWNT/PAni 1:96 and (e) SWNT/PAni 1:144.

predominant. Finally, the formation of large plates of randomly distributed polyaniline nanofibers can be observed at higher SWNTs/PAni ratios (Fig. 1(e)). The SWNTs are well-dispersed in all the nanocomposites, causing the polyaniline to spread throughout the film, resulting in a more accessible area.

Through the TEM images of the neat SWNT and SWNT/PAni 1:16 and 1:96 nanocomposites (Fig. 2(a)–(c), respectively), it is possible to confirm the randomly and interconnected arrangement of the SWNTs. Also is possible observe the polyaniline covering the CNT bundles in the nanocomposites. Small particles of the catalyst can also be observed in all the SWNT-containing samples, once the SWNTs have been used without any previous treatment.

The Raman spectra of the SWNTs and the nanocomposites, collected with a laser emitting at 632.8 nm, are shown in Fig. 3(a). The SWNT spectrum (Fig. 3(a–I)) shows two dominant features: the radial breathing modes (RBM) at approximately  $200\text{--}290\text{ cm}^{-1}$  and the G-band, which is divided into  $G^+$  ( $1593\text{ cm}^{-1}$ ) and  $G^-$  ( $1556\text{ cm}^{-1}$ ), associated with the vibrations of the carbon atoms along the nanotube axis and in the circumferential direction, respectively. Other observed bands include the disorder-induced D-band ( $1310\text{ cm}^{-1}$ ) and the second-order overtone 2D (or  $G'$ ) band ( $2610\text{ cm}^{-1}$ ) [29,30]. The Raman spectrum of the neat PAni shows the characteristic profile of emeraldine salt, as can be seen in the Fig. S2 [27,31–33]. The PAni obtained in the nanocomposites (Fig. 3(a) II–IV) presented two different vibrational behaviors from the neat PAni (Fig. 3(b)). First, a band shift of  $1168\text{ cm}^{-1}$  to  $1173\text{ cm}^{-1}$  was observed for all the nanocomposites. This shift indicates that the SWNTs stabilize the PAni in the polaronic form of the emeraldine salt. The second difference is the absence of some bands in the nanocomposites spectra that correspond to the cross-linked portion ( $577, 1393$  and  $1643\text{ cm}^{-1}$ ), indicating that the SWNTs avoid (or prevent) the PAni reticulation. The same behavior was also observed for MWNT/PAni nanocomposites synthesized by the interfacial method [22].

The electronic behavior of the thin films was characterized by UV–Vis spectroscopy (Fig. 4(a)). An intense band at  $281\text{ nm}$  is observed in the UV–Vis spectra of the SWNTs (Fig. S3), assigned to  $\pi\text{--}\pi^*$  transition of the carbon nanotubes, besides the interband transitions for metallic ( $400\text{--}650\text{ nm}$ ) and semiconducting ( $550\text{--}900\text{ nm}$ ) SWNTs [34,35]. The UV–Vis spectrum of the neat PAni confirms that it is in the emeraldine salt form, with bands at  $348\text{ nm}$ , corresponding to the  $\pi\text{--}\pi^*$  transition (valence to conduction transition band), and at  $446\text{ nm}$  and a broad band at approximately  $756\text{ nm}$ , both corresponding to the transition of the valence to polaronic band [33,36,37]. In all the nanocomposites, the PAni is also observed in its emeraldine salt form, and the electronic transition of the polaronic band (at  $756\text{ nm}$ ) is shifted to a higher wavelength (particularly in the SWNTs/PAni 1:96), indicating that the SWNTs induce a more delocalized polaronic structure of the PAni [33,38]. Pictures of a very thin and transparent film of the SWNTs/PAni 1:96 nanocomposite deposited over a flexible

substrate, as well as of the SWNTs and all the SWNTs/PAni nanocomposites prepared in this work deposited over glass substrates, can be seen in Fig. S4.

The thickness of the nanocomposite films was dependent on the SWNTs/aniline ratio, with values at approximately  $89 \pm 24$ ,  $127 \pm 22$  and  $246 \pm 65\text{ nm}$  for the samples SWNTs/PAni 1:16, 1:96 and 1:144, respectively. All the nanocomposites were very thin, indicating that the interfacial system is an excellent way to produce films on the nanoscale. The films of neat PAni and SWNTs displayed a thickness of approximately  $306 \pm 56$  and  $98 \pm 25\text{ nm}$ , respectively.

Basic electrochemical characterization was performed by CV and charge/discharge measurements, which are presented in Fig. 5. Both neat PAni and the nanocomposites presented the characteristic peaks of the conducting polymer, thereby confirming the electro activity of the polyaniline (Fig. 5(a)). The redox pairs assigned to the leucoemeraldine/emeraldine ( $A/A'$ ) and emeraldine/permigraniline ( $D/D'$ ) conversion are observed at approximately  $0.2\text{ V}$  and  $0.85\text{ V}$ , respectively, for all samples. The intermediate redox pairs ( $B/B'$  and  $C/C'$ ) corresponding to the ortho-coupled polymer or products of degradation of the PAni are also observed [39,40]. In the voltammograms of all the nanocomposites, a peak at approximately  $0.92\text{ V}$  is observed, unlike for the neat PAni, indicating that the presence of the SWNTs in the nanocomposites stabilize the conducting polymer in the emeraldine form, making the formation of the permigraniline form difficult [22]. This electrochemical behavior can be attributed to the SWNTs stabilizing the polaronic structure of the emeraldine salt, which is responsible for the increased oxidation resistance of the PAni to its permigraniline form, as observed from the higher oxidation potential in the nanocomposites. Furthermore, the nanocomposite SWNTs/PAni 1:96 presented a higher current density, even though it has fewer aniline moieties than the 1:144 nanocomposite. This behavior can be attributed to all the electroactive material in the 1:144 nanocomposite not being used due to the formation of a thick layer of PAni (as seen by SEM) that precludes penetration of the electrolyte [41].

The volumetric specific capacitance for the nanocomposites and for neat PAni was calculated from equation (1):

$$Cv = (t \times i) \div (\Delta E \times v) \quad (1)$$

where  $Cv$  is the volumetric specific capacitance ( $\text{F cm}^{-3}$ ),  $t$  is the discharge time (s),  $i$  is the applied charge/discharge current (A) and  $\Delta E$  is the variation of the potential (V) during discharge [42]. The specific capacitance was calculated by volume because this feature is most significant for a thin film pseudo-capacitor, while a mass assessment could be estimated by an unconventional method. The  $Cv$  in the second charge/discharge cycle was  $38.09, 184.75, 34.91$  and  $29.90\text{ F cm}^{-3}$  for the composites with SWNTs/PAni ratios of 1:16, 1:96, 1:144 and for neat PAni, respectively (Fig. 5(b)). These

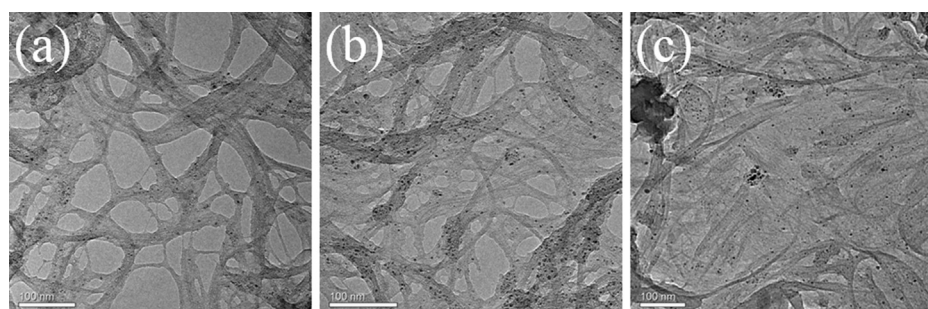
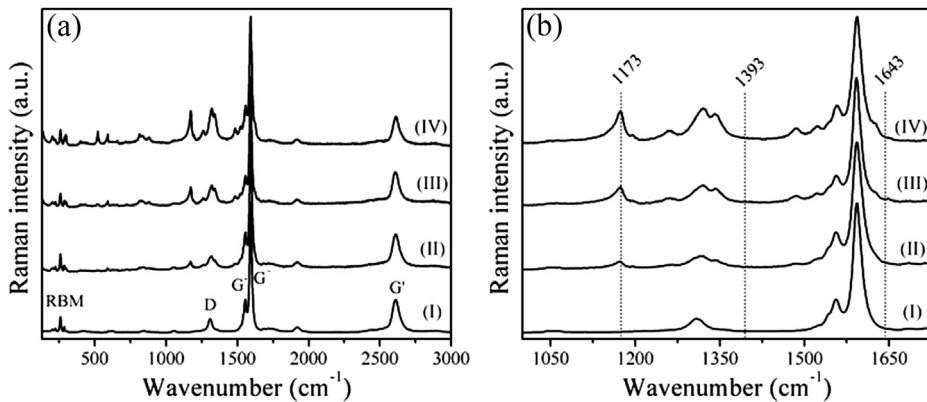


Fig. 2. TEM images of the samples: (a) SWNT, (b) SWNT/PAni 1:16 and (c) SWNT/PAni 1:96.



**Fig. 3.** (a) Raman spectra (1.96 eV) of the samples: (I) SWNT; (II) SWNT/PAni 1:16; (III) SWNT/PAni 1:96 and (IV) SWNT/PAni 1:144; (b) details of the Raman spectra between 1000 and 1725  $\text{cm}^{-1}$ .

differences in the  $C_V$  of the nanocomposites can be explained according to the SWNTs/aniline ratio, in which the sample with the lower SWNTs/aniline ratio (SWNT/PAni 1:16) has a small pseudo-capacitance, while that with a ratio of 1:96 presented a higher charge/discharge time (Fig. 5(c)). In the composites with higher SWNTs/PAni ratios, the excess polymer decreases the pseudo-capacitance, a behavior that can be attributed to the hindrance of the electrolyte permeation through the active material due to the existence of a shell of PAni, as confirmed by the SEM and CV results. Furthermore, the  $C_V$  of the SWNTs/PAni 1:96 nanocomposite compared to that of the neat PAni (which contains the same amount of aniline) is 6 times higher, indicating that the presence of SWNTs improves the capacitance because for several reasons, such as the presence of pores between the carbon nanotubes that facilitate the electrolyte permeation during the charge/discharge process and the excellent conductivity and interconnectivity credited to the SWNTs [41–43].

Considering that the connectivity and the porosity of the carbon nanotubes network are strictly dependent on their dimensions (aspect ratio), the volumetric specific capacitance of the SWNTs/PAni 1:96 composite was compared with two other composites synthesized with a commercial sample of multiwall carbon nanotubes (MWNTs<sub>commercial</sub>) and a home-made multiwall carbon nanotubes

filled with an iron species (MWNTs-Fe) [26] using the same amount of aniline as in the SWNTs/PAni 1:96 sample. Comparing the three samples of carbon nanotubes, the aspect ratio decreases in the following manner: SWNTs > MWNTs<sub>commercial</sub> > MWNTs-Fe. The thicknesses of these nanocomposite thin films were  $168 \pm 42$  and  $411 \pm 100$  nm for the MWNTs<sub>commercial</sub> and MWNTs-Fe, respectively, with  $C_V$  values of 66.80 and  $33.95 \text{ F cm}^{-3}$  (Fig. 6(a)), respectively. Although the charge/discharge time of the MWNTs-Fe/PAni nanocomposite was higher than the one synthesized with the MWNTs<sub>commercial</sub> (Fig. 6(b)), its  $C_V$  was smaller due to its large thickness. The  $C_V$  of the SWNTs/PAni nanocomposite was superior when compared to the MWNT samples. Such behavior can be attributed to the different aspect ratios of the carbon nanotubes. Because the SWNTs have a higher aspect ratio, a higher number of tube/tube connections is expected, enhancing the network porosity [44] and resulting in a hybrid material with improved conductivity and more accessible pores for intercalation and depletion of charges. Although the SWNTs arrange themselves into bundles, they provide more current-carrying channels due to the elevated number of carbon nanotubes on the surface [45].

The influence of the number of layers of SWNTs/PAni 1:96 deposited over glass substrates (and neat PAni for comparison) on the capacitive properties were investigated by galvanostatic charge/discharge measurements. The charge/discharge time of the nanocomposite was directly proportional to the number of layers deposited over the substrate (Fig. 6(c)). For neat PAni, the charge/discharge time increased up to two layers, but no significant increase is observed in the third layer, indicating a possible obstruction of the electrolyte motion. As expected, the thickness of the nanocomposite increases with the number of layers. The values found were approximately  $173 \pm 14$ ,  $416 \pm 80$  and  $533 \pm 69$  nm for 1, 2 and 3 layers of nanocomposite, while for neat PAni, the values were approximately  $328 \pm 33$ ,  $567 \pm 167$  and  $680 \pm 96$  nm for 1, 2 and 3 layers, respectively. The volumetric specific capacitance of the nanocomposite remained practically unchanged, despite the number of thin layers, indicating that the porous structure of the nanocomposite produced by the interfacial method was maintained, allowing the properties of the thin film to manifest three-dimensionally.

A digital picture of the SWNTs/PAni pseudo-capacitor can be observed in Fig. 7(a). A very thin and transparent film deposited over the flexible substrate is observed. The thickness of the device can be attributed to the substrate and the electrolyte, and the pseudo-capacitor shows a high flexibility when twisted or folded.

The electrochemical behavior of the all-solid capacitor in the presence of SWNTs/PAni thin films was completely different than

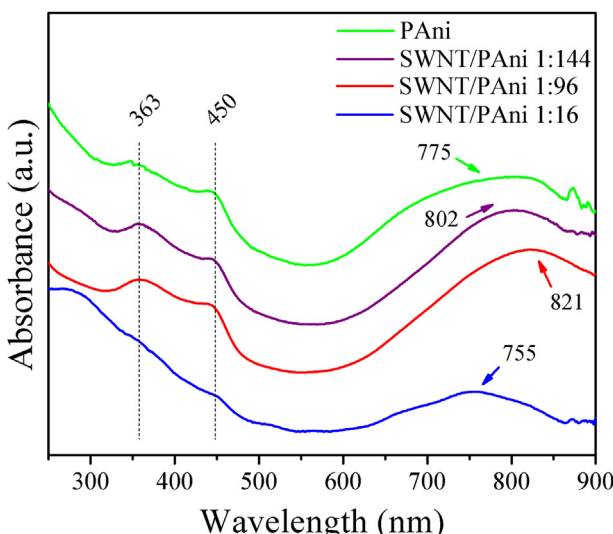


**Fig. 4.** UV-Vis spectra of the samples.

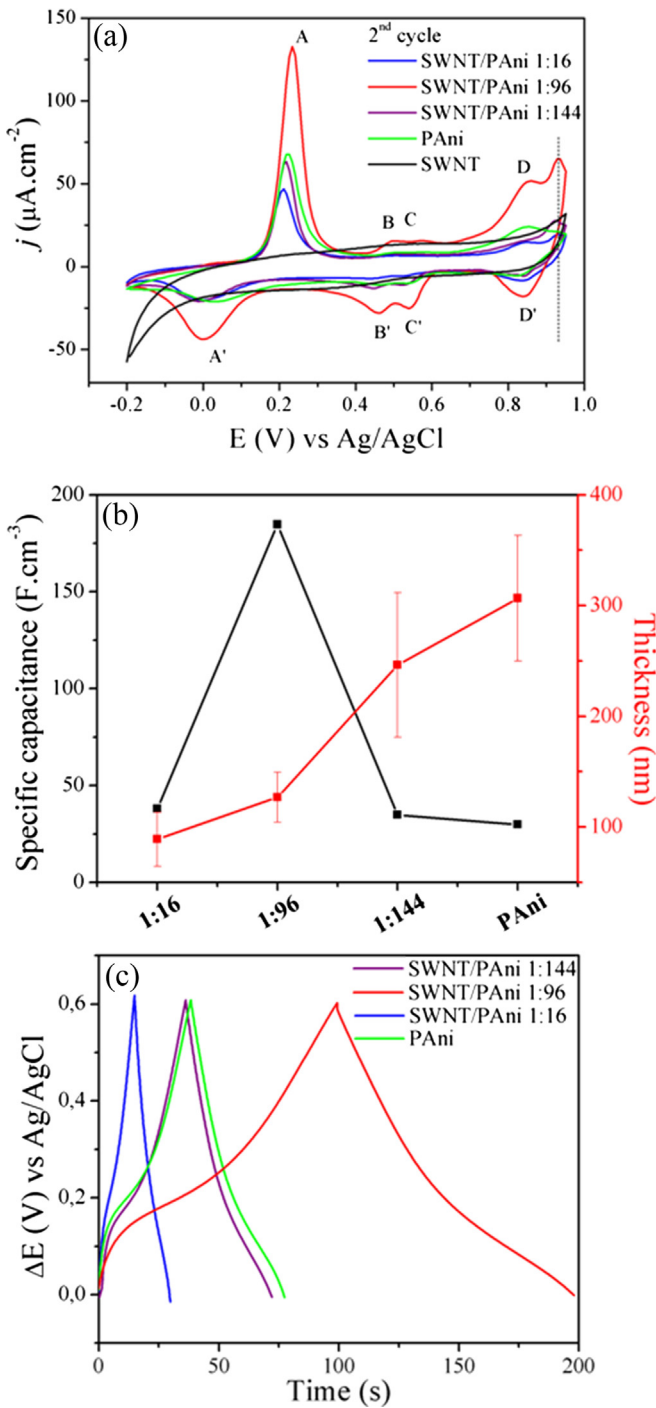


**Fig. 5.** (a) CV curves in the range of  $-0.2$ – $0.95$  V at scan speed of  $20$   $\text{mV}\cdot\text{s}^{-1}$ ; (b) specific capacitance ( $\text{F}\cdot\text{cm}^{-3}$ ) and thickness (nm) for samples with different SWNT/aniline ratios and (c) charge/discharge times for samples with different SWNT/aniline ratios.

the control device, built with only electrolyte sandwiched between the two plastic substrates (Fig. 7(b)). In the cyclic voltammetric curve of the control sample, no pseudo-capacitive behavior is observed, while in the SWNTs/PANI, a capacitive current is evidenced, with the presence of two redox pairs. This behavior indicates that even though the CV of the all-solid device is different than the electrode in solution, the SWNT/PANI still shows pseudo-capacitive behavior. The electrochemical behavior was affected

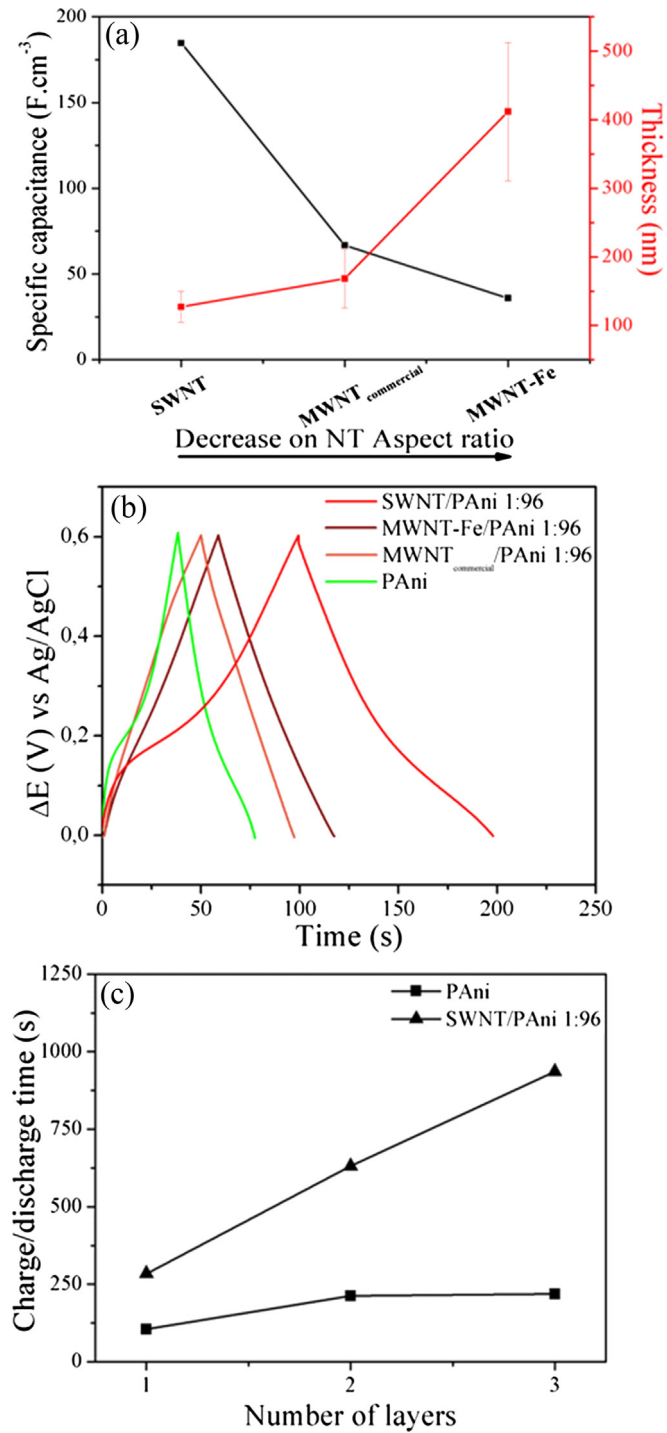


**Fig. 6.** (a) Specific capacitance ( $\text{F}\cdot\text{cm}^{-3}$ ) and thickness (nm) and (b) charge/discharge times for samples obtained with different CNT; (c) the dependence of charge/discharge time for the number of layers of PANI and SWNT/PANI 1:96.

during and after mechanical deformation (twisting process), as shown in the profile of the CV curves (Fig. 7(c)). The two redox pairs that are not clearly observed when the device is straight ( $\Delta E_p = 0.104$  V) are more defined during and after the twisting process. During the twisting process, the two redox pairs are more separated ( $\Delta E_p = 0.16$  V), indicating a more difficult redox process. After the mechanical deformation, the two redox pairs remain well-defined, with lower  $\Delta E_p$  values ( $\Delta E_p = 0.085$  V), indicating a higher

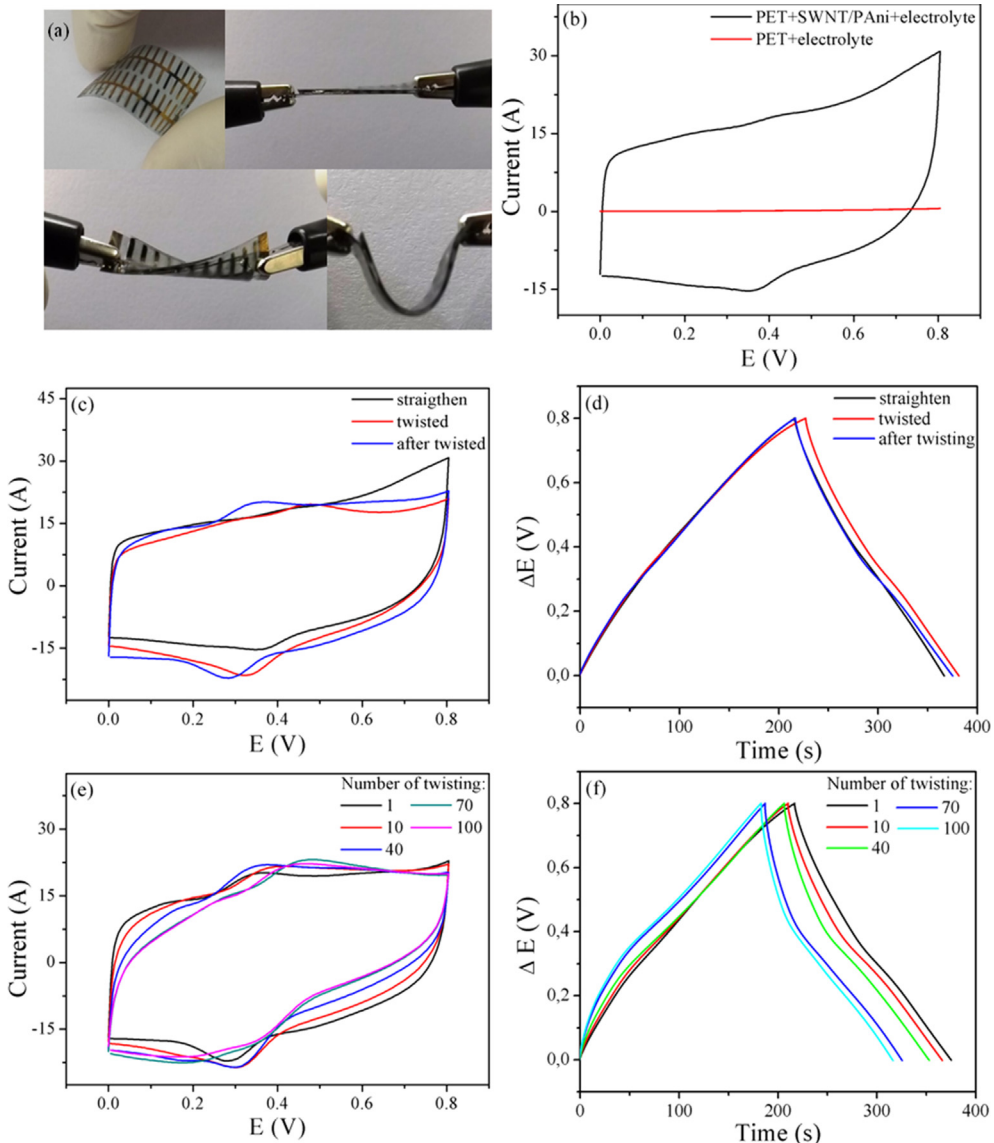


**Fig. 7.** (a) Digital images of the SWNT/PAni 1:96 nanocomposite deposited over PET and the all-solid device straighten, twisted and folded; (b) CV curves in the range of 0–0.8 V at scan speed of  $10 \text{ mV s}^{-1}$  of the devices with and without SWNT/PAni 1:96 nanocomposite; (c) charge/discharge galvanostatic measure of the device; (d) CV curves of the device over different mechanical deformations; (e) CV and (f) CD curves of the device for different numbers of mechanical deformations.

reversibility of the redox process. The charge/discharge profile of the device was almost the same as that of the nanocomposite in aqueous solution (Fig. 7(d)). The charge/discharge time was unchanged in the three configurations (straight, twisted and after twisting), indicating that the pseudo-capacitive behavior was maintained. The volumetric specific capacitance after twisting was  $76.7 \text{ F cm}^{-3}$ . The CV and charge/discharge profiles over subsequent mechanical deformations were slightly changed (Fig. 7(e) and (f), respectively). In the CV, the same profile is retained until after 40 processes of deformation, and then  $\Delta E_p$  increased. The charge/discharge time remained approximately 360 s, dropping to 312 s after 100 twisting processes. A decrease of 16% in the volumetric specific capacitance was observed, indicating a short reduction in the capacitive properties of the SWNTs/PAni device. This behavior, however, should be more associated to problems related to the electrolyte (loss of adherence or conductivity) than to the nanocomposite itself. The charge-discharge stability of the all-solid device (straighten) was maintained in 88% after 1000 cycles (Fig. S5).

The electrochemical impedance spectroscopy (EIS) was employed to the SWNT/PAni 1:96 nanocomposites (over the FTO

electrode and the all-solid device) once this is a powerful technique to evaluate the impedance resistance in electrochemical systems. Both Nyquist plots (Fig. 8(a)) present an arc instead a semicircle in the high frequency region, which can be attributed to a low electronic resistance due to the presence of SWNT [46–48]. The Warburg impedance (which is frequently observed as a straight line with slope of  $45^\circ$ ) is not clearly seen in Fig. 8(a). This result indicates a very small resistance (in high frequency) due to the movement of ions from the electrolyte to the porous structure of the nanocomposite [49]. The EIS curves for both the FTO electrode and all-solid device present a vertical line in low frequency with a fast increase of the imaginary part, indicating a high capacitive behavior and ion diffusion on the structure of the nanomaterial [11,48,49]. The equivalent circuit of the Fig. 8(b), was used as model to calculate the value of charge-transfer resistance ( $R_{ct}$ ) and the contact/electrolyte resistance ( $R_s$ ). This circuit presents the contribution of both the double-layer and the pseudocapacitive behavior. The  $R_s$  value found for the nanocomposite over FTO electrode was  $50.3 \Omega$ , and for the nanocomposite in the all-solid capacitor was  $604 \Omega$ , The difference can be attributed to the partially insulating

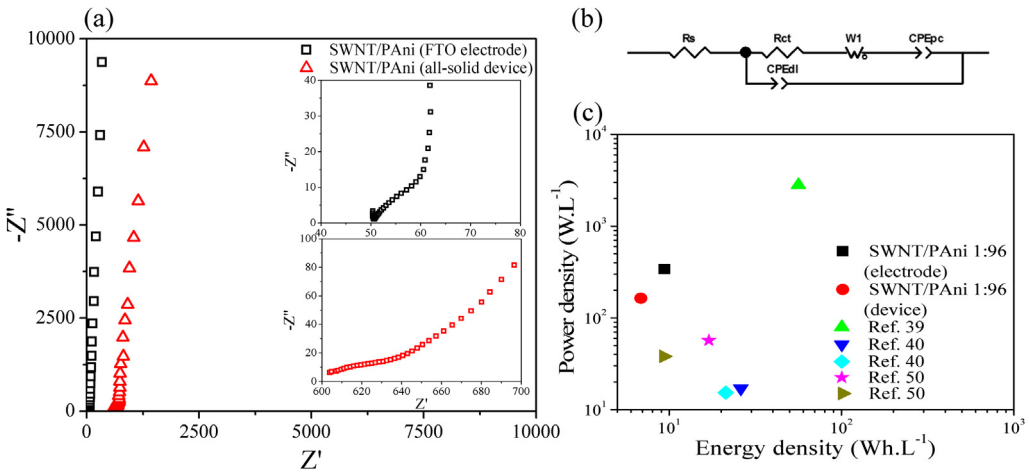


Fig. 8. (a) Nyquist plot for SWNT/PAni electrode and all-solid capacitor, (b) the equivalent circuit model and (c) the Ragone plot.

substrate along with a low permeable gel electrolyte (PVA) in the solid state device. On the other hand, the EIS analysis presents lower values of  $R_{ct}$  for both FTO electrode ( $4.8 \Omega$ ) and the all-solid device ( $23.2 \Omega$ ), indicating the good conductivity and a great reversibility of the faradaic reactions for SWNT/PAni nanocomposites [49].

The best values reported here for the volumetric specific capacitance of both the electrode ( $184.75 \text{ F cm}^{-3}$ ) and the all-solid capacitor ( $76.7 \text{ F cm}^{-3}$ ) are very promising results compared with other systems previously reported, such as hierarchical structures of graphene/polyaniline/carbon nanotubes ( $188 \text{ F cm}^{-3}$ ) and graphene/polyaniline ( $153 \text{ F cm}^{-3}$ ) composites [42], multi-walled carbon nanotubes/polyaniline/MnO<sub>2</sub> ternary coaxial nanostructures ( $296 \text{ F cm}^{-3}$ ) [50], layer-by-layer structures of MWNTs/graphene oxide ( $58 \text{ F cm}^{-3}$ ) and MWNTs/chemically reduced graphene ( $144 \text{ F cm}^{-3}$ ) [51] and polypyrrole/carbon nanotubes ( $67 \text{ F cm}^{-3}$ ) and polypyrrole/carbon nanotubes between graphene nanosheets ( $122 \text{ F cm}^{-3}$ ) [52], even though high values of the volumetric specific capacitance have been reported for polyaniline/carbon nanotube array (PAni/CNTA) composite electrodes (approximately  $500 \text{ F cm}^{-3}$ ) [41]. The retention of the capacitive behavior of the all-solid device (84%) after 100 mechanical deformations (twisting process) is also interesting compared to other all-solid devices such as MWNTs/PAni (92% after 50 bending cycles) [16] and MnO<sub>2</sub>/CNTs (99% after 100 bending cycles) [17]. The energy and power density (Ragone plot) of the SWNT/PAni nanocomposite and the comparison to similar materials reported in literature are plotted in the Fig. 8(c), showing promising results.

The great novelty of the all-solid capacitor prepared in the present work compared to other devices, even though it is not completely optimized, is the use of a novel and a very thin and freestanding film of SWNTs/PAni nanocomposite, starting from a small amount of reactants. The liquid–liquid interface methodology adopted to prepare the nanocomposite thin films allows their deposition over a myriad of plastics substrates, as well as the establishment of different architectures for the devices, thereby establishing a new concept for ultrathin capacitors.

#### 4. Conclusions

The synthesis and characterization of SWNTs/PAni nanocomposites through interfacial polymerization, as well as the pseudo-capacitive behavior of these films, have been reported and discussed in this paper. The method presented here is a simple way to obtain a very thin and freestanding film that can be directly

deposited over different substrates. The presence of the SWNTs in the nanocomposites clearly improves the pseudo-capacitive properties of the PAni, even when compared with other types of carbon nanotubes. The manufacturing of a thin and flexible all-solid device from SWNTs/PAni nanocomposites indicates the great potential of this methodology in the field of capacitors and to produce these nanomaterials as integrated parts of ultrathin electronic devices.

#### Acknowledgments

Authors acknowledge the financial support from CNPq, CAPES, NENNAM (Pronex, Fundação Araucária/cnpq), National Institute of Science and Technology of Carbon Nanomaterials, and CME-UFPR for the TEM images. VHRDS acknowledge CAPES for the fellowship.

#### Appendix A. Supplementary data

Supplementary data related to this article can be found at <http://dx.doi.org/10.1016/j.jpowsour.2014.02.070>.

#### References

- C. Peng, S. Zhang, D. Jewell, G.Z. Chen, *Prog. Nat. Sci.* 18 (2008) 777–788.
- G.A. Snook, P. Kao, A.S. Best, *J. Power Sources* 196 (2011) 1–12.
- M. Inagaki, H. Konno, O. Tanaike, *J. Power Sources* 195 (2010) 7880–7903.
- O. Kimizuka, O. Tanaike, J. Yamashita, T. Hiraoka, D.N. Futaba, K. Hata, K. Machida, S. Suematsu, K. Tamamitsu, S. Saeki, Y. Yamada, H. Hatori, *Carbon* 46 (2008) 1999–2001.
- K.S. Ryu, K.M. Kim, N.G. Park, Y.J. Park, S.H. Chang, *J. Power Sources* 103 (2002) 305–309.
- S. Sivakkumar, W.J. Kim, J. Choi, D.R. Macfarlane, M. Forsyth, D.W. Kim, *J. Power Sources* 171 (2007) 1062–1068.
- G. Yu, X. Xie, L. Pan, Z. Bao, Y. Cui, *Nano Energy* 2 (2013) 213–234.
- R. Ramya, R. Sivasubramanian, M.V. Sangaranarayanan, *Electrochim. Acta* 101 (2013) 109–129.
- B. Dong, B.L. He, C.L. Xu, H.L. Li, *Mat. Sci. Eng. B* 143 (2007) 7–13.
- G. Zhou, D. Wang, F. Li, L. Zhang, Z. Weng, H. Cheng, *New Carbon Mater.* 26 (2011) 180–186.
- Z. Niu, P. Luan, Q. Shao, H. Dong, J. Li, J. Chen, D. Zhao, L. Cai, W. Zhou, X. Chen, S. Xie, *Energy Environ. Sci.* 5 (2012) 8726–8733.
- Y.K. Zhou, B.L. He, W.J. Zhou, J. Huang, X.H. Li, B. Wu, H.L. Li, *Electrochim. Acta* 49 (2004) 257–262.
- C. Meng, C. Liu, L. Chen, C. Hu, S. Fan, *Nano Lett.* 10 (2010) 4025–4031.
- J. Ge, G. Cheng, L. Chen, *Nanoscale* 3 (2011) 3084–3088.
- C. Meng, C. Liu, S. Fan, *Electrochim. Commun.* 11 (2009) 186–189.
- H. Lin, L. Li, J. Ren, Z. Cai, L. Qiu, Z. Yang, H. Peng, *Nature* 3 (2013) 1353.
- Y.J. Kang, H. Chung, W. Kim, *Synth. Met.* 166 (2013) 40–44.
- Y.J. Kang, S.J. Chun, S.S. Lee, B.Y. Kim, J.H. Kim, H. Chung, S.Y. Lee, W. Kim, *ACS Nano* 6 (2012) 6400–6406.
- Y.J. Kang, H. Chung, C.H. Han, W. Kim, *Nanotechnology* 23 (2012) 065401.
- M.F. El-Kady, V. Strong, S. Dubin, R.B. Kaner, *Science* 335 (2012) 1326–1330.

[21] E. Skovroinski, R.J. de Oliveira, A.J.G. Zarbin, A. Galembeck, *Synth. Met.* 159 (2009) 2309–2311.

[22] R.V. Salvatierra, M.M. Oliveira, A.J.G. Zarbin, *Chem. Mater.* 22 (2010) 5222–5234.

[23] R.V. Salvatierra, C.E. Cava, L.S. Roman, A.J.G. Zarbin, *Adv. Funct. Mater.* 23 (2013) 1490–1499.

[24] S.H. Domingues, R.V. Salvatierra, M.M. Oliveira, A.J.G. Zarbin, *Chem. Commun.* 47 (2011) 2592–2594.

[25] M.C. Schnitzler, M.M. Oliveira, D. Ugarte, A.J.G. Zarbin, *Chem. Phys. Lett.* 381 (2003) 541–548.

[26] J. Huang, R.B. Kaner, *J. Am. Chem. Soc.* 126 (2004) 851–855.

[27] G.M. do Nascimento, P.Y.G. Kobata, M.L.A. Temperini, *J. Phys. Chem. B* 112 (2008) 11551–11557.

[28] S. Xing, H. Zheng, G. Zhao, *Synth. Met.* 158 (2008) 59–63.

[29] M.S. Dresselhaus, G. Dresselhaus, A. Jorio, A.G. Souza Filho, R. Saito, *Carbon* 40 (2002) 2043–2061.

[30] M.S. Dresselhaus, G. Dresselhaus, R. Saito, A. Jorio, *Phys. Rep.* 409 (2005) 47–99.

[31] J.E.P. da Silva, S.I.C. de Torresi, D.L.A. de Faria, M.L.A. Temperini, *Synth. Met.* 101 (1999) 834–835.

[32] J.E.P. da Silva, D.L.A. de Faria, S.I.C. Torresi, M.L.A. Temperini, *Macromolecules* 33 (2000) 3077–3083.

[33] R.V. Salvatierra, L.G. Moura, M.M. Oliveira, M.A. Pimenta, A.J.G. Zarbin, *J. Raman Spectrosc.* 43 (2012) 1094–1100.

[34] Y. Maeda, S. Kimura, M. Kanda, Y. Hirashima, T. Hasegawa, T. Wakahara, Y. Lian, T. Nakahodo, T. Tsuchiya, T. Akasaka, *J. Am. Chem. Soc.* 127 (2005) 10287–10290.

[35] Y. Tian, H. Jiang, J. Pfaler, Z. Zhu, A.G. Nasibulin, T. Nikitin, B. Aitchison, L. Khriachtchev, D.P. Brown, E.I. Kauppinen, *J. Phys. Chem. Lett.* 1 (2010) 1143–1148.

[36] W. Huang, A. Macdiarmid, *Polymer* 34 (1993) 1833–1845.

[37] G.M. do Nascimento, T.B. Silva, P. Corio, M.S. Dresselhaus, *J. Raman Spectrosc.* 41 (2010) 1587–1593.

[38] A.G. Macdiarmid, A.J. Epstein, *Synth. Met.* 69 (1995) 85–92.

[39] A. Zhang, C. Cui, J.Y. Lee, *Synth. Met.* 72 (1995) 217–223.

[40] A.R. Elkais, M.M. Gvozdenović, B.Z. Jugović, J.S. Stevanović, N.D. Nikolić, B.N. Grgur, *Prog. Org. Coat.* 71 (2011) 32–35.

[41] H. Zhang, G. Cao, W. Wang, K. Yuan, B. Xu, W. Zhang, J. Cheng, Y. Yang, *Electrochim. Acta* 54 (2009) 1153–1159.

[42] X. Lu, H. Dou, S. Yang, L. Hao, L. Zhang, L. Shen, F. Zhang, X. Zhang, *Electrochim. Acta* 56 (2011) 9224–9232.

[43] V. Gupta, N. Miura, *Electrochim. Acta* 52 (2006) 1721–1726.

[44] L.F.C. Pereira, M.S. Ferreira, *Nano Commun. Networks* 2 (2011) 25–38.

[45] L.F.C. Pereira, C.G. Rocha, A. Latgé, J.N. Coleman, M.S. Ferreira, *Appl. Phys. Lett.* 95 (2009) 123106–123109.

[46] H.J. Choi, I.Y. Jeon, S.W. Kang, J.B. Baek, *Electrochim. Acta* 56 (2011) 10023–10031.

[47] M. Liu, Y.-E. Miao, C. Zhang, W.W. Tjiu, Z. Yang, H. Peng, T. Liu, *Nanoscale* 5 (2013) 7312–7320.

[48] J. Kang, J. Wen, S.H. Jayaram, X. Wang, S.-K. Chen, *J. Power Sources* 234 (2013) 208–216.

[49] Q. Cheng, J. Tang, N. Shinya, L.-C. Qin, *J. Power Sources* 241 (2013) 423–428.

[50] Q. Li, J. Liu, J. Zou, A. Chunder, Y. Chen, L. Zhai, *J. Power Sources* 196 (2011) 565–572.

[51] H.R. Byon, S.W. Lee, S. Chen, P.T. Hammond, Y. Shao-Horn, *Carbon* 49 (2011) 457–467.

[52] X. Lu, H. Dou, C. Yuan, S. Yang, L. Hao, F. Zhang, L. Shen, L. Zhang, X. Zhang, *J. Power Sources* 197 (2012) 319–324.